MECHANISMS OF IMPROVED OIL RECOVERY FROM SANDSTONE BY LOW SALINITY FLOODING

Munish Kumar[1,2], Andrew Fogden[2], Norman R. Morrow[3] and Jill S. Buckley[3]
[1]DigitalCore, Australian National University, Canberra, Australia
[2]Dept. of Applied Mathematics, Australian National University, Canberra, Australia
[3]Dept of Chemical and Petroleum Engineering, University of Wyoming, Laramie, WY

ABSTRACT

Oil recovery mechanisms in four Berea sandstones were probed by flow experiments in mini-plugs and analysis of registered images of the resulting distributions of mineral components and oil deposits in pores in the before and after states. After single-phase flow of brine, from high to low salinity, x-ray μ-CT was able to resolve some slight differences in mineral distribution in pores, while SEM imaging of cut faces more clearly showed the migration of clay particles and other fines. Two-phase experiments involved drainage of high salinity brine by crude oil, followed by aging and flooding by high or low salinity brine. Using the SEM technique, fines migration was observed to be greater than for the single-phase experiments, even for the traditional case of high salinity connate and injected brine. Low salinity flooding gave even greater movement of fines, although in all systems the changes were presumed to be insufficient to drastically alter overall rock permeability. SEM images typically show migrated fines intermingled with the oil deposits. The overall amount of oil deposits from spectroscopy also increases from high to low salinity flooding. Results are interpreted in terms of the moving oil-brine meniscus stripping loosely bound clays and other fines, which can lower its interfacial tension and increase its stability and ability to sustain flow paths for oil recovery.

INTRODUCTION

There is widespread interest in the mechanism by which oil recovery is increased by either displacing oil with low salinity brine at high initial oil saturation or by mobilization of residual oil established by high salinity flooding. Laboratory results indicate the onset of increased recovery by low salinity flooding, if observed, occurs at less than 4000 ppm. The cut-off is not well defined and is dependent on specific components of the brine and the properties of the rock and crude oil. Tang and Morrow [1] concluded that increased recovery from sandstone by low salinity flooding requires the presence of clay, an initial water saturation, and crude oil. Later, study of displacement of refined oil from mixed wet rocks showed that the presence of the crude oil-brine interface is also necessary [2]. The sufficient conditions are still unknown, as evidenced by examples of lack of increase in oil recovery when all necessary conditions are fulfilled (e.g., [3]). In the clay-bearing sandstones first investigated in [1], increase in effluent pH was observed and ascribed to clay ion exchange. However, effluent interfacial tensions were diminished by less than

30% from ~25 dynes/cm, insufficient for improved recovery by lowering the ratio of capillary to viscous forces [4]. Further, for many subsequently investigated crude oil-brine-rock (COBR) combinations which responded to low salinity flooding, effluent pH ranged from a little below to just above neutral.

Tang and Morrow [1] noted that increased recovery was accompanied by production of water-wet fine particles that sank to the bottom of the oil-water separator, and the possible presence of partially oil-wet fines in a small rag layer between produced oil and brine. It was hypothesized that improved oil recovery involved the release of mixed-wet fines from pore walls, possibly together with dislodgement of water-wet particles. However, for many COBR combinations, production of fines in the effluent was not observed, and accordingly, Lager et al. [5] argued that the increased oil recovery did not involve their movement. Dissolution of rock minerals was also discounted as a feasible explanation. However, the mechanism of dissolution depends on the rock mineralogy [6-7]. On the basis of detailed on-line analysis of effluent brine composition, Lager et al. [5] concluded that the low salinity recovery mechanism depended on detachment of crude oil from rock surfaces by multi-component ion exchange. The present work addresses the same oil-brine combinations and similar Berea sandstones for which variable low salinity response was observed in previous core flooding experiments [8]. The current study focuses on tracking changes in location of fines and deposited organic material including asphaltenes that accompany injection of brine and reduction in its salinity.

PROCEDURES
Rocks and Fluids
Cores, of diameter ~38 mm and length ~77 mm, of four Berea types, denoted B1-B4, were selected. Table 1 lists their properties, either measured on the core material or from literature data on sister cores. Sample B1 is from the same batch of standard Berea denoted Berea 500 (absolute permeability ~500 mD) in Zhang and Morrow [8], while B4 is from the batch of low permeability Berea denoted Berea 60 [8].

The crude oil and brines were the same as those used by Zhang and Morrow [8], for which the average oil recovery values from high and low salinity waterflooding listed in Table 1 pertain. The asphaltic crude oil was from the Minnelusa field in Wyoming, with density 0.9062 gcm^{-3}, viscosity 77.2 mPa.s, n-C_7 asphaltene content 9.0 wt%, and acid and base numbers 0.17 and 2.29 mg KOH/g oil (all at room temperature) [9]. The crude oil was filtered prior to use. The high salinity brine, of composition matching the Minnelusa formation [8], was prepared by dissolving 28.99 g NaCl, 2.79 g $CaCl_2.2H_2O$, 1.42 g $MgCl_2.6H_2O$ and 6.90 g Na_2SO_4 (all analytical grade) in 1 L of deionized water from a Millipore Milli-Q system (as used throughout). The low salinity brine was a 100-fold dilution of this. Its total dissolved salt content of 387 ppm is lower than that of many low salinity floods in the literature, however its use facilitates comparison with Zhang and Morrow [8]. Both brines were used at their natural pH ~6.0 after vacuum degassing.

Table 1. Porosity, absolute permeability, specific surface area, cation exchange capacity, and relative abundance of kaolinite (K), illite (I) and chlorite (C) from x-ray diffraction, for the 4 Berea samples, together with their average oil recovery by high or low salinity waterflooding [8].

Berea type	ϕ (%)	K (mD)	BET (m^2/g)	CEC (meq/100g)	clays	R_{wf} High (%OOIP)	R_{wf} Low (%OOIP)
B1	21.5	680	0.851	0.196	K > I > C	65.1	81.5
B2	22.8	290			K > C > I		
B3	24.6	320					
B4	20.5	30	1.150	0.290	K = C > I	74.1	72.6

Preparation of Mini-plugs

A total of 8 mini-plugs were prepared by dry coring, with 7 having diameter and length ~8 and 20 mm, and the eighth, from Berea B1, with diameter and length ~5 and 15 mm. An inert fluoropolymer tube was heat shrunk to tightly envelop the walls of each core, using a heat gun at 130 ^{o}C. The 7 larger mini-plugs were crosswise cut wet into two equal halves using a Struers blade. The halves were lightly placed back together, with cut faces facing, in a specially designed core holder fitted to a flow cell connected to a motorized syringe pump. 75 PV of toluene, 50/50 toluene/methanol (v/v), and methanol were successively injected through each mini-plug to flush contaminants. Each mini-plug was then lightly vacuum dried at 60 ^{o}C. In this clean "before" state the two faces of the mini-plugs were SEM imaged, also verifying that their faces were free of debris from cutting.

Flow Experiments

A total of 8 experiments of two types was carried out, namely single-phase high-to-low salinity brine flooding of the 8 mm mini-plugs for Berea samples B1, B3 and B4 and the uncut 5 mm B1 mini-plug, and two-phase secondary oil recovery by either high or low salinity waterflooding for both of the 8 mm mini-plugs for samples B1 and B2. All brine and oil injections were performed at a flow rate of ~1x10^{-3} cm^{3}s^{-1}. After SEM imaging the faces of each mini-plug, the two parts were set face to face in the holder. This was connected to the cell and pump, and injected with 35 PV of the high salinity brine, after which the flow cell was immersed in a bath of the brine and degassed under very light vacuum for ~1-2 h. The cell was reattached to the pump for injection of 10 PV of this brine, then locked-in to equilibrate for 12-24 h. For the two-phase experiments, the mini-plug was then drained to breakthrough by injection of 20 PV of crude oil at 70-75 ^{o}C; the cell was then sealed and aged in a 75 ^{o}C oven for 3 days. The subsequent flooding, with low salinity brine for the single-phase experiments and either brine for two-phase experiments, comprised injection of 20 PV at 65-70 ^{o}C, followed by a 10 min. shut-in, then a second 20 PV brine injection. For two-phase experiments, residual crude oil was removed by injection of 100 PV of decalin at 65-75 ^{o}C until the effluent was colorless, followed by 50 PV of heptane at 25 ^{o}C to remove the maltene fraction of oil deposits. In all cases, 75 PV of methanol at 25 ^{o}C was then injected to remove salt. The mini-plug was removed from its holder and its halves were immersed in clean decalin for 30 min., followed by heptane for 10 min. (for two-phase experiments only), then in 77.5/22.5 methanol/water (v/v) at 65 ^{o}C for 4 days to dissolve remaining salt, followed by vacuum

drying at 25 ^{o}C. The two faces of the mini-plugs were then SEM imaged in this "after" state. Imaging verified that the methanol/water bath had no effect on rock or oil deposits.

Analysis by SEM and X-ray μ-CT
Each half of the 7 mini-plugs, before and after the above-mentioned experiments, was stood in a sample holder with cut face upwards and horizontal, and imaged with a field emission scanning electron microscope (FESEM, Zeiss UltraPlus Analytical) under high vacuum in secondary electron mode at 1 kV. The low voltage allowed high resolution (3072x2304 pixel) imaging without any sample treatment (e.g. conductive sputter coating), with only occasional beam charging artifacts. The protocol is illustrated in Fig. 2a; a series of 18 micrographs at magnification 303x was acquired, traversing the cut face from edge to edge and back again. For each image, a higher magnification (3110x) close-up was taken, focusing on a pore of interest. In the "after" state the stage was rotated until the region near the heat shrink boundary corresponding to the first "before" image was located, then the same set of 18 low and 18 high magnification images was acquired. Quartz grains are unmoved by the experiments, so their size and shape enable matching of "before" and "after" locations without physical marking. For the two-phase samples, even higher magnification (9970x) images of oil deposits in the "after" state were taken.

As a complement, the ANU x-ray μ-CT facility [10] was used to 3D image the 5 mm mini-plug of Berea B1 without cutting or emptying of its fluids. The mini-plug was imaged in its clean, dry state prior to the single-phase experiment, and in its wet states after high salinity infiltration and after low salinity flooding. In all cases, the central 6 mm region of the mini-plug was imaged, with the tomograms composed of 2048^3 voxels at a resolution of 2.97 μm/voxel. A registration algorithm [11] was used to superpose, at voxel resolution, images in these different states.

Spectroscopy of Oil Deposits
For each of the 4 mini-plugs after the two-phase experiments and SEM imaging, a 4 mm-thick section was wet cut from the end of the plug half which faced the injection inlet (where oil tends to build-up heavily), and discarded. Each half, after removal of its heat shrink, was then separately crushed with mortar and pestle, and placed in a bath of 10 g decalin for 18 h. to strip any remaining unbound oil components from the rock powder, then decanted and replaced by 6 g heptane for 6 h. to strip residual maltenes, again decanted, and the powder dried in a 50 ^{o}C oven. To each known mass of rock powder, a known mass (~7 g) of 87.3/12.7 (w/w) azeotropic chloroform/methanol mixture [12] was added to dissolve the asphaltene-based deposits, then decanted after 18 h. The asphaltene solutions from each mini-plug half were analyzed with a UV-visible scanning spectrophotometer (Shimatzu UV-3101PC) to quantify their absorbance over the interval 200-800 nm. Calibration standards were obtained by heptane precipitation and separation of the asphaltene fraction of the crude oil, followed by dissolving the asphaltenes in the azeotropic mixture to concentrations in the range 0.4-4 x10^{-3} wt%. The absorbance of the standards at 520 nm exhibited Beer-Lambert linear dependence, from which the percentage mass of asphaltene per dry rock mass was derived for each mini-plug half.
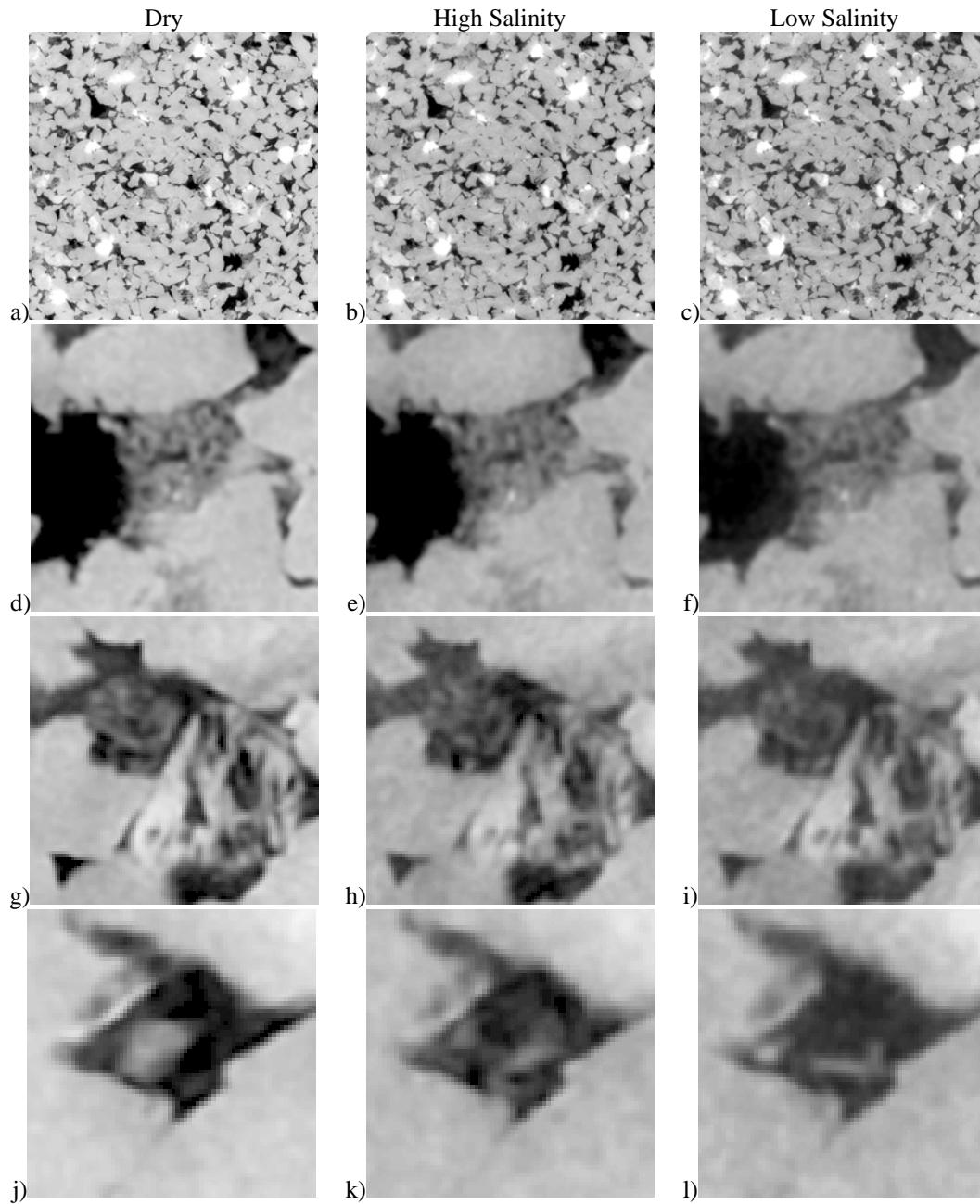
Figure 1. Corresponding slice subsets of Berea sample B1 in the dry state (left column), after high salinity infiltration (middle), and subsequent low salinity flooding (right). Square edge lengths are: a)-c) 3.26 mm, d)-f) 344 μm, g)-i) 306 μm, and j)-l) 214 μm.

RESULTS AND DISCUSSION
X-ray μ-CT of Single-Phase System
Figure 1 shows 2D subsets of the reconstructed tomograms of the 5 mm B1 mini-plug, registered in its 3 states (columns) of the single-phase experiment and with increasingly smaller fields of view (rows). In the largest field of Figs. 1a-c, little if any difference is

apparent, with the same being true of the close-up of a clay-filled pore in Figs. 1d-f. The subarea in Figs. 1g-i features another clay-filled pore and a weathered grain, possibly with slight alteration close to voxel resolution. In the highest close-up of a filled pore in Figs. 1j-l, changes are apparent due both to high salinity infiltration and subsequent low salinity flooding. However, specifics of these structural changes are difficult to resolve. Quantification of changes would necessitate image segmentation, which is challenging for Berea itself due to its mixture of clay types and distributions. These uncertainties would be greater than the low degree of small-scale changes actually taking place. Thus, in these situations μ-CT requires support from higher resolution techniques.
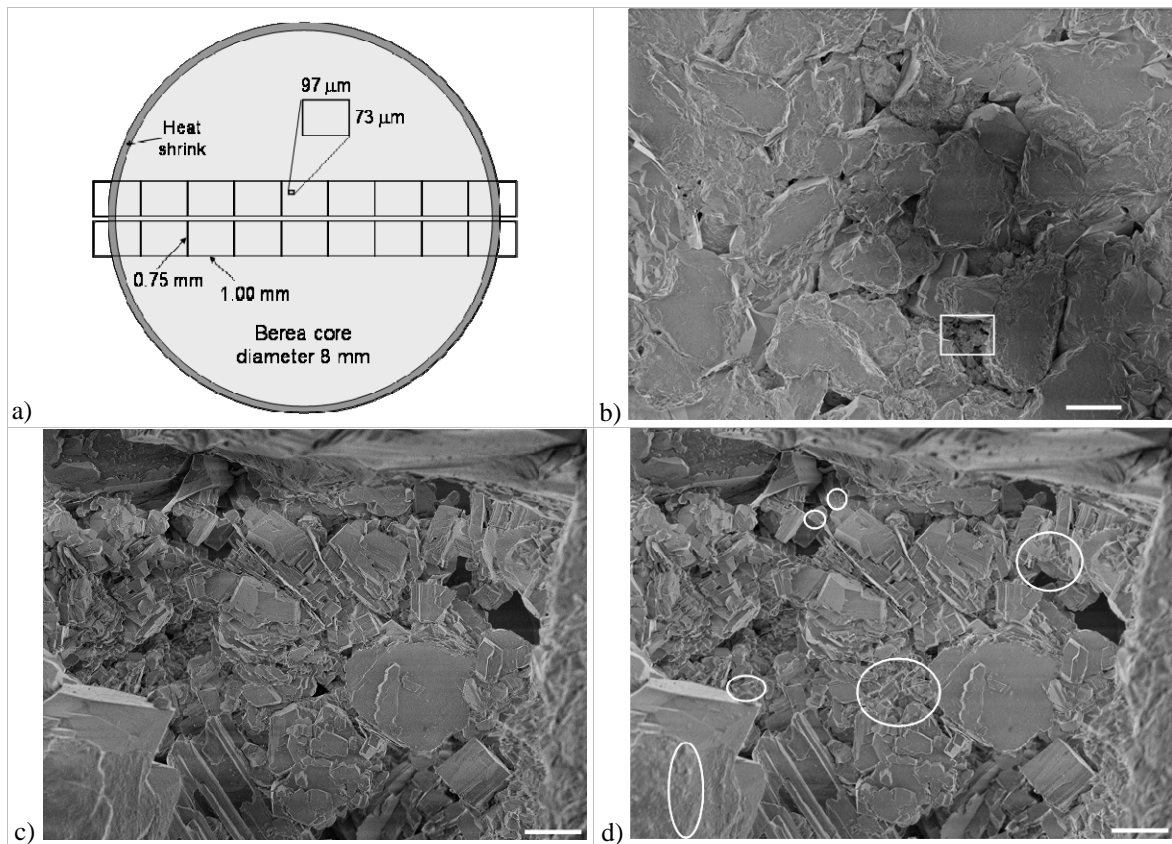

Figure 2. a) Diagram of FESEM image acquisition procedure, and b)-d) micrographs of Berea sample B1: b) the "before" state at low magnification (scale bar 100 μm), with white rectangle showing location of the c) subarea at high magnification (scale bar 10 μm); d) the corresponding subarea after high-to-low salinity single-phase flooding, with white ellipses encircling regions in which changes from c) to d) are apparent.

SEM of Single-Phase Systems

Figure 2 displays SEM images of the cut face of B1 from before and after single-phase flooding for the same rock and states as compared in the left and right columns of Fig. 1. Figure 2b shows a typical low magnification micrograph, i.e. a 1.00×0.75 mm^2 rectangle in the series of 18 for each face in Fig. 2a. (The dark cloud across its lower right is due to beam charging.) The surface quartz grains have been cleanly cut, while the pore bodies

and throats between and below them remain untouched. Viewed at this size, the "after" counterpart of Fig. 2b (not shown) is practically identical, as is true for the vast majority of pairs for all 7 systems. Instances of grain removal, due to contact of the faces during assembly and disassembly in the core holder, amount to only approx. 0.1% of all grains inspected, although naturally higher near the plug edges. For this reason only the middle 7 images per row in Fig. 2a, i.e. 28 per mini-plug sample, were analyzed. Occasional changes in particle features intermediate to grain and clay sizes are observed in all 7 systems, which could be handling damage or truly in response to fluid flow. Digital zooming of these low magnification images reveals, however, a far more ubiquitous sub-texture of changes at or below clay particle size. Despite these images having resolution of 0.32 μm/pixel, these small-scale changes can typically only be resolved by comparing the higher magnification images obtained by focusing on a single pore framed by surrounding grains, e.g. the "before" and "after" pair in Figs. 2c and d. Thus for each system studied, the comparison reduced to assessment of the differences in these 28 pairs of close-ups. In all cases, overall similarities between "before" and "after" states are prevalent, i.e. while almost all pores exhibit change, none are altered beyond recognition, and no throats become substantially blocked or unblocked. Indeed, considering low and high magnification images, the alteration of the original rock permeability is presumably not major. As SEM images are 2D, some information in pores is lost, e.g. obscured by grain overhangs, due to the slight differences in planarity on mounting the halves "before" and "after". Thus, the image analysis involved manually encircling each altered subarea, fitting an ellipse to the projected area of altered mineral features (excluding gaps in between), and summing each to obtain the total change per image area and its average over all 28 micrographs. Further, altered features are binned into two categories, defining "small" as changes comprising small particles or clusters of them (e.g. all in Fig. 2d fit this category), and "large" reserved for single particle events > 5 μm diameter (e.g. the grain edge broken-off from Fig. 3c to d in the circled area). The latter are far less common; in all 7 systems, the total of "small" and "large" changes number 1584 and 69. For the pair in Figs. 2c and d, the "small" changes amount to 4.6% of the image area.

Figure 4a plots the averaged changes thus obtained in these two categories for the samples on which single-phase experiments were performed. There is a weak trend to increased total changes with decrease in both permeability and response of oil recovery to low salinity flooding (Table 1). However, for all 3 rocks the dominant "small" category of changes lies in the range 1.5-2.5%, and should be regarded as very similar. Further, for these 3 samples the nature of changes is similar, rarely involving movement of the identifiable clay which fills pores (and often appears orthogenically intergrown), but rather resulting from movement and deposition of smaller particles about and on this fixed porous matrix. Mobile particles at the top end of this size range, e.g. the right-most ellipse in Fig. 2d, are typically crystalline, either platy clay particles or of more blocky form. Frequently the change is manifested as an aggregate of submicron particles, e.g. the bottom left ellipse in Fig. 2d, difficult to individually resolve at this magnification. The particle in the top left ellipse of Fig. 2d, which has only moved slightly, is an exception; the vast majority of small changes are not traceable, originating from other pores.
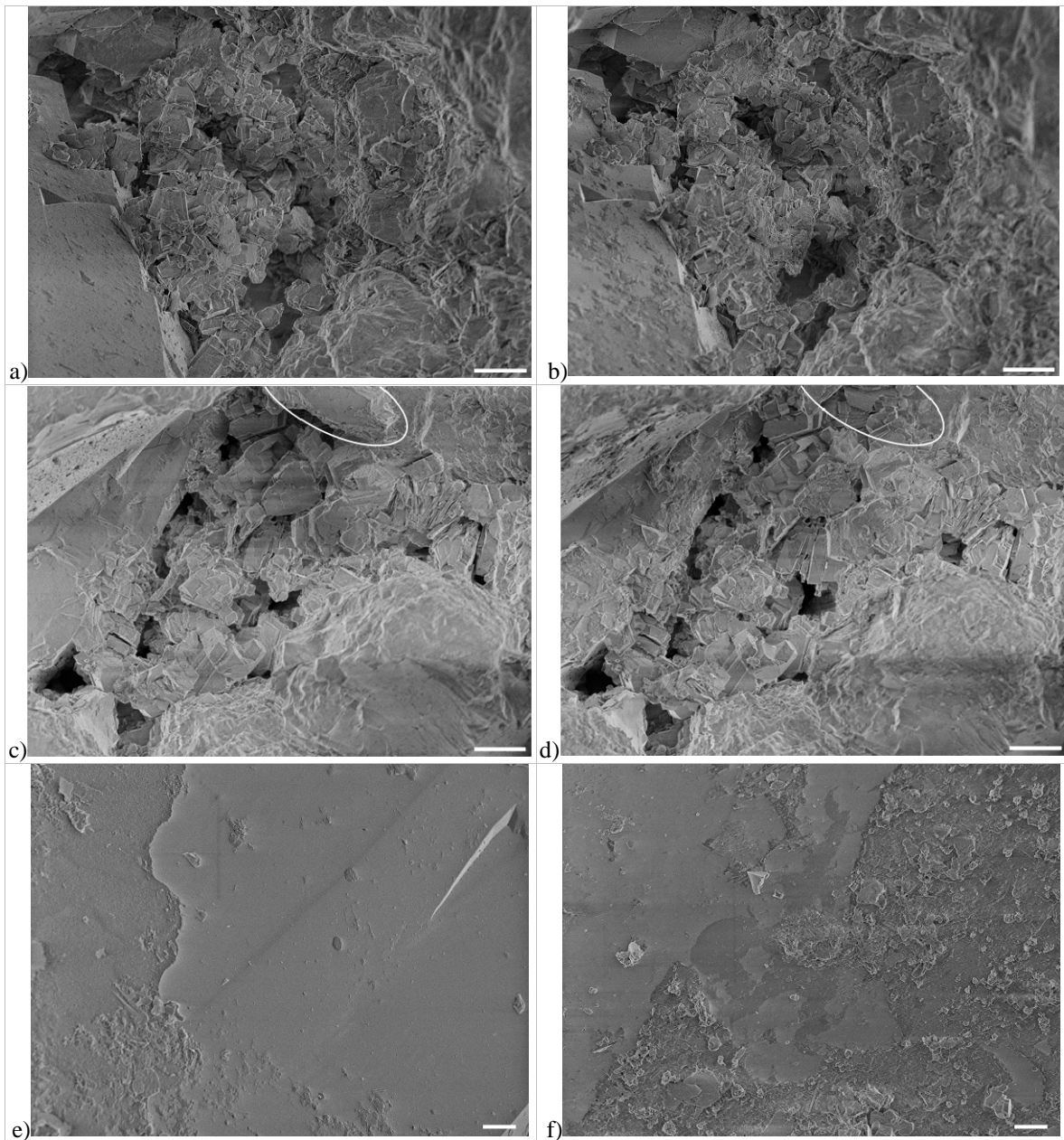
Figure 3. a)-d) FESEM high-magnification (scale bar 10 μm) sub-area pairs of Berea sample B1 in: a) the "before" state and b) after oil recovery by high salinity flooding; c) the "before" state and d) after oil recovery by low salinity flooding. e)-f) Higher magnification (scale bar 2 μm) close-ups of different quartz overgrowth areas of Berea B1, showing oil deposits after recovery by e) high or f) low salinity flooding.

SEM of Two-Phase Systems

Examples of high-magnification pairs for B1 after oil recovery by high or low salinity flooding are given in Figs. 3a-b and c-d, respectively, with the former exhibiting 4.5% of "small" changes and the latter having 9.4% of "small" and 2.4% of "large" changes. The corresponding averages over all 28 pairs for B1 and B2 are graphed in Fig. 4b. Changes

only include mineral phase; a rock surface bearing an asphaltene film devoid of relocated particles of angular form is not counted. Despite this, the "small" change exceeds all single-phase systems in Fig. 4a, even for high salinity flooding in which the rocks were never exposed to low salinity brine. Hence for traditional flooding to recover oil from sandstone reservoirs behaving as standard Berea, small mineral fines migrate in an amount equivalent to ~4% of projected pore cross-sectional area. Low salinity recovery for both samples leads to more than twice the change of their high salinity counterparts.
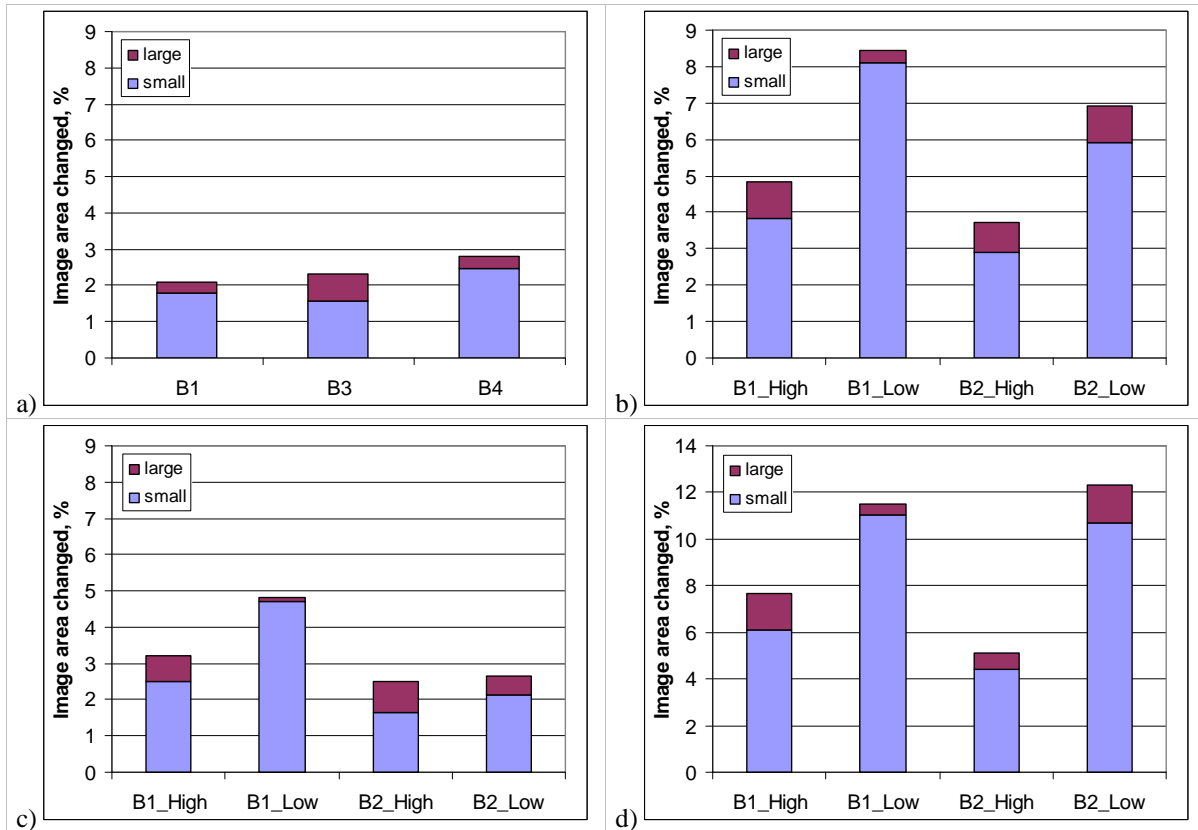

Figure 4. Average percentage of FESEM high-magnification image areas altered from "before" to "after" states, divided into small-scale changes and large single-particle changes, for a) high-to-low salinity single-phase floods in 3 Berea samples and b) oil recovery by high or low salinity flooding for 2 samples. c) and d) separately count the predominately c) water-wet or d) oil-wet (deposition) environments comprising b).

In all 4 cases, most pores imaged remain water-wet in their clay-filled centres; deposition of asphaltene films in tightly curved interstices of the immobile clay networks (or within feldspar grains) is relatively rare. Rather, oil deposits generally occur on grain walls of sufficiently low curvature to permit oil entry, in line with mixed-wet expectations. Grain surfaces at lower left in Fig. 3b and upper left in 3d are examples of this. Significantly, these asphaltene films on grains are often associated with small mineral fines not present in the "before" state, which are the principal source of the increased change in the two-phase systems. This migration of fines with the oil is especially prevalent for low salinity flooding. Figures 3e and f show representative higher-resolution images of oil deposits on

different smooth quartz overgrowths after high or low salinity flooding, respectively. The areas without asphaltene film, to the right in Fig. 3e and upper left in 3f, are mainly free from fines, while the deposited areas are greatly enriched in fines, more so for the low salinity case. Changes also occur in the substantially water-wet clay networks, in the form of migration of individual small particles and clusters, as for the single-phase systems, together with migrated agglomerates of small fines and oil residues.

Each image pair was simply categorized as either oil- or water-wet, by whether or not the pore's grain walls are substantially covered by asphaltene film, and the averages in Fig. 4b were decomposed into the separate water-wet and oil-wet averages in Figs. 4c and d. (No presumption is made as to the degree of oil wetness, or that the advancing contact angle exceeds 90°.) Change within oil-wet environments greatly exceeds its water-wet counterpart for both samples and salinities, and the trend of increased change for low over high salinity perseveres in both graphs. Changes in Fig. 4c are generally of similar size to the single-phase systems in Fig. 4a, although the former are overestimates of a completely water-wet ideal, since most images contain some oil deposit with associated mineral fines which inflate the total change, especially for B1 at low salinity in Fig. 4c.
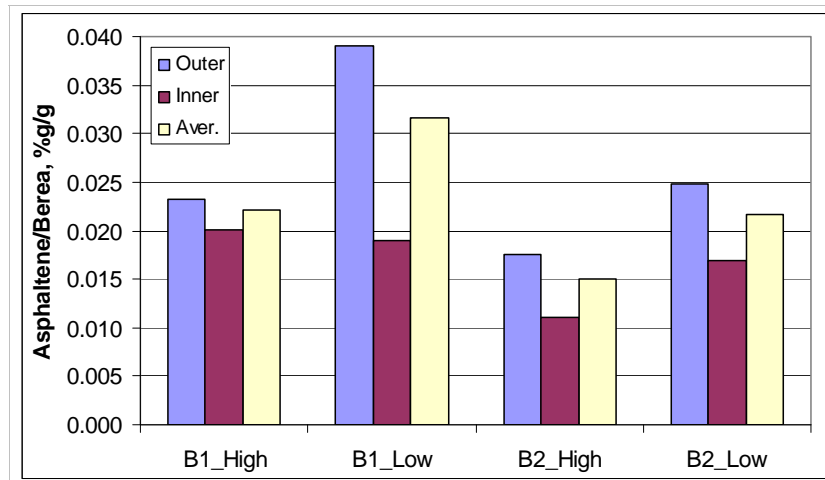

Figure 5. Mass percentage of asphaltene on rock from spectroscopy of deposits extracted after oil recovery by either high or low salinity flooding for 2 Berea samples.

Oil Deposit Amounts

Although the SEM technique can resolve the changes in mineral structure, and image analysis gives some statistical quantification of trends, ability to discern and quantify asphaltene-based deposits by SEM is more limited, aside from situations where films lie on overgrowths and/or contain mineral fines. To complement this limited information, extraction of the deposits and analysis by UV-visible spectroscopy gives their overall amount, with the results plotted in Fig. 5. The average percentage mass of asphaltene per mass of mini-plug rock is partnered by the corresponding fractions for the mini-plug half closest to the oil and brine inlet face ("Inner" in Fig. 5) and outlet face ("Outer"). The overall average mass fraction clearly increases from high to low salinity for both samples,

and is systematically higher for B1. Trends are thus similar to those for overall mineral change in Fig. 4b. The deposit mass fraction from the outer half has this same behavior, while the inner half is lower, and less dependent on salinity, at least for B1. Deposit fraction should not be taken as a direct indicator of wettability; it cannot be simply concluded that low salinity flooding leads to a more oil-wet final state than high salinity, as rock area coverage of deposit is unknown. Moreover, the lesser deposition closer to the oil inlet is the reverse of the usual wettability gradient from restoration by one-ended oil injection. Figures 4 and 5 support the view that fines migrate with the oil during its recovery, and more so for low salinity flooding. The higher deposition in this case presumably derives from the increased fraction of fines rendered oil-wet by oil exposure, and which migrate downstream to skew the deposit distribution towards the outlet.

Interpretation of Mechanisms

Single-phase results directly evidence that, while most clay particles and fines in these sandstones remain immobile during low salinity flooding, a small but significant fraction migrate. This involves poorly bonded particles in pores and lining walls, from platy clay of diameter several μm to submicron fines. Migration can involve individual particles or aggregates, and spans more than one pore. While no single-phase flows with only high salinity brine were performed, analysis of water-wet pores in two-phase systems suggests that small particle mobilization also occurs in this case, although less so than for low salinity. Low salinity increases electrostatic repulsion between particles and with walls to aid mobilization by the shear force of brine flow. For two-phase systems, oil advance during drainage to initial water saturation provides the extra interfacial tension force to further strip pore-lining fines, even those thinly sheathed by brine. These particles may enter the oil bulk, although they presumably have a greater tendency to reside at the oil-brine interface to reduce its energy. Oil aging will render the particles partially or completely oil-wet. On flooding, the particle-stabilized interface will enhance recovery by decreasing snap-off, aided and replenished by further particles removed from walls by the moving meniscus, or diffusing to it through bulk brine in throats. Low salinity raises the likelihood of stripping from brine-sheathed walls and mobilization in brine-filled throats. Rock wettability may not change during recovery if originally water-wet regions lined or filled with particles remain water-wet. As oil passes through pores, some interfacial fines are shed and dumped on grains, as seen in most SEM images. If this turnover continues during recovery, the particle fraction in recovered oil will be small.

CONCLUSION

A SEM technique was developed to supplement μ-CT capabilities to obtain registered images of rock cores before and after flow processes. While necessitating cutting and fluid flushing, it gives deeper insight into changes in inorganic and organic phase distributions on scales down to submicron. Recovery from Berea by traditional flooding was shown to be accompanied by migration of fines in quantities sufficient to have some bearing on oil-brine interfacial stability, and that low salinity flooding increases this tendency, in line with Tang and Morrow [1]. While other mechanisms may contribute to oil recovery, the consequences of this mobilization should be further addressed.

ACKNOWLEDGEMENTS

REFERENCES

1. Tang, G.Q., Morrow, N.R. "Influence of Brine Composition and Fines Migration on Crude Oil/Brine/Rock Interactions and Oil Recovery", *J. Pet. Sci. Eng.* (1999) **24**, 99-111.
2. Zhang, Y., Xie, X., Morrow, N.R. "Waterflood performance by injection of brine with different salinity for reservoir cores", paper SPE 109849 presented at the 2007 ATCE, Anaheim, 11-14 Nov.
3. Skrettingland, K., Holt, T., Tweheyo, M.T., Skjevrak, I. "Snorre Low Salinity Water Injection - Core Flooding Experiments and Single Well Field Pilot", paper SPE 129877 presented at the 2010 SPE IOR Symp., Tulsa, 24-28 Apr.
4. Tang, G.Q., Morrow, N.R. "Injection of Dilute Brine and Crude Oil/Brine/Rock Interactions", *Geophysical Monograph 129*, American Geophysical Union, 2002, 171-179.
5. Lager, A., Webb, K.J., Black, C.J.J., Singleton, M., Sorbie, K.S. "Low Salinity Oil Recovery - An Experimental Investigation", paper SCA 2006-36 presented at the 2006 SCA Internat. Symp., Trondheim, 12-16 Sept.
6. Pu, H., Xie, X., Yin, P., Morrow, N.R. "Application of Coalbed Methane Water to Oil Recovery from Tensleep Sandstone by Low-Salinity Waterflooding", paper SPE 113410 presented at the 2008 SPE IOR Symp., Tulsa, 19-23 Apr.
7. Lebedeva, E., Senden, T.J., Knackstedt, M., Morrow, N.R. "Improved Oil Recovery from Tensleep Sandstone - Studies of Brine-Rock Interactions by Micro-CT and AFM", paper presented at the 15th European Symp. of IOR, Paris, 27-29 Apr., 2009.
8. Zhang, Y., Morrow, N.R. "Comparison of Secondary and Tertiary Recovery with Change in Injection Brine Composition for Crude Oil/Sandstone Combinations", paper SPE 99757 presented at the 2006 IOR Symp., Tulsa, 22-26 Apr.
9. Tie, H.G., Tong, Z.X., Morrow, N.R. "The Effect of Different Crude Oil/Brine/Rock Combinations on Wettability Through Spontaneous Imbibition", paper SCA 2006-02 presented at the 2003 SCA Internat. Symp., Pau, Sept 21-24.
10. Sakellariou, A., Sawkins, T., Senden, T., Limaye, A. "X-ray Tomography for Mesoscale Physics Applications", *Physica A* (2004) **339**, 152-158.
11. Latham, S., Varslot, T., Sheppard, A. "Image Registration: Enhancing and Calibrating X-ray Micro-CT Imaging", paper SCA2008-35 presented at the 2008 SCA Symp., Abu Dhabi, 29 Oct.-2 Nov.
12. Dubey, S.T., Waxman, M.H. "Asphaltene Adsorption and Desorption From Mineral Surfaces", *SPE Res. Eng.* (1991), August, 389-395.